Journal of Membrane Science 663 (2022) 120979

Contents lists available at ScienceDirect

Journal of Membrane Science

journal homepage: www.elsevier.com/locate/memsci

Dynamic scouring of multifunctional granular material enhances filtration performance in membrane bioreactor: Mechanism and modeling

Wenxiang Zhang [b,*], Wenzhong Liang [a,**], Zhien Zhang [c]

[a] State Environmental Protection Key Laboratory of Water Environmental Simulation and Pollution Control, South China Institute of Environmental Sciences, Ministry of Ecology and Environment of the People's Republic of China, Guangzhou, 510530, PR China
[b] Biological and Environmental Science and Engineering Division, Water Desalination and Reuse Research Center, King Abdullah University of Science and Technology, Thuwal, Saudi Arabia
[c] Department of Chemical and Biomedical Engineering, West Virginia University, 40110 Evansdale Drive, Morgantown, WV, 26506, USA

ARTICLE INFO

Keywords:
Membrane bioreactor (MBR)
Granular material
Dynamic scouring mechanism
Membrane fouling control
Threshold flux
Membrane cleaning

ABSTRACT

The granular material (GM) is able to effectively improve the membrane fouling control in membrane bioreactor (MBR) by dynamic scouring, adsorption behavior and enzymatic degradation. However, their roles and effects on the filtration performance of MBR remain unclear. The present work investigated the GM dynamic scouring mechanism, revealed the multifunctional quantitative evaluation, and clarified the filtration performance at various GM operating conditions in MBR. First, the aerobic granular sludge (AGS)-filtration process was still limited by the presence of irreversible membrane fouling, which decreased the filtration performance in MBR (threshold flux [169.5 L m^{-2} h^{-1}] and (turning point of membrane fouling resistance [1.1×10^{12} m^{-1}]). To solve this problem, the GMs (activated carbon [AC] and laccase immobilized activated carbon [LAC]) was added into the AGS-filtration process to enhance the filtration performance. Above all, based on momentum conservation, the dynamic scouring mathematical model was put forward to elucidate the dynamic scouring mechanism of GM towards the membrane surface. The scouring stress on the membrane surface was proportional to the total mass of GM and offered an additional shear effect for clearly promoting the collision between GM and foulant, and decreasing their deposition on the membrane surface via friction with the membrane. Then, both AC and LAC exhibited a highly desirable adsorption efficiency for foulant removal, whereas the enzymatic degradation of LAC also furtherly straightened this effect. Furthermore, a new contribution quantification model was proposed for evaluating the contribution rates of dynamic scouring (59.1%), adsorption behavior (36.4%) and enzymatic degradation (4.6%) to boost the filtration performance, implying that the dynamic scouring and adsorption behavior brought about the dominated promotion. At the GM of 8 g/L and size of 300–600 μm, AGS-filtration exhibited an optimized performance in term of threshold flux, turning point of membrane fouling resistance and membrane cleaning. The present study offers insights into the mechanism that GM multifunctional scouring enhanced filtration performance in MBR.

1. Introduction

Membrane fouling of membrane bioreactor (MBR), significantly affected by the interactions between the sludge and membrane, greatly increases the operating cost and weakens the filtration efficiency [1]. Beyond question, membrane fouling, has been, and continuous to be, one of the main obstacles for the further wide application of MBR. Sludge, as a highly complex system, consists of various organic substances, cells, salts, colloids, extracellular polymeric substances (EPS) and sludge flocs [2]. All these substances are identified as the potential membrane foulants, and can be effectively controlled via hydrodynamic enhancement, which is an efficient method to in current MBR engineering.

The hydraulic shear generated by aeration, as the mainstream hydrodynamic enhancement technology, can create an invisible barrier between the membrane and sludge, reducing the membrane foulant deposition, while providing the sufficient oxygen for biochemical degradation [3,4]. However, the long-term aeration operation in MBR

* Corresponding author.
** Corresponding author.
E-mail addresses: zhangwenxiang6@hotmail.com, wenxiang.zhang@kaust.edu.sa (W. Zhang).

https://doi.org/10.1016/j.memsci.2022.120979
Received 20 July 2022; Received in revised form 2 September 2022; Accepted 3 September 2022
Available online 9 September 2022

actual engineering brings about the serious energy consumption, which even accounts for about 40% of the operating cost [1]. Reducing the aeration demand and improving membrane fouling control become the future development goals of MBR [5]. Optimizing the aeration device location and aeration condition can promote the shear stress on the membrane surface at a lower aeration rate [6,7]. But it is difficult to efficiently decrease the energy consumption and control the membrane foulant produced by soluble organic matters such as EPS and SMP only through hydraulic shear aeration [2]. Besides, the intermittent filtration and backwash are also able to mitigate membrane fouling via decreasing the filtration load and timely removing membrane foulant [8]. Nevertheless, these hydrodynamic enhancement strategies affect the filtration efficiency and need a higher equipment requirement [9], as well as increase the operating cost [10]. Seeking more efficient hydrodynamic enhancement strategies for reducing energy cost and improving efficiency is a critical development direction for promoting the filtration performance of MBR.

The sludge granulation is another promising hydrodynamic enhancement strategy [11]. Through sludge granulation, the aerobic granular sludge (AGS) formed and reinforced the shear stress using its dynamic scouring via its large particle size, thus MBR exhibited the high permeability (>2-6-fold) and low membrane fouling (0.1 kPa/day) [12]. However, in the long-term operation, AGS-MBR still suffers membrane fouling and flux decline [13]. Elevating the critical point of irreversible fouling can prolong the duration of high filtration efficiency in AGS-MBR. Increasing the granulation ratio is conducive to promote the dynamic scouring effect and shear stress. However, the excessive AGS concentration may cause sludge disintegration, aggravating the membrane fouling. As a result, adding granular material (GM) in AGS-MBR can reduce the AGS concentration and raise the particle ratio [14,15], avoiding the disintegration risk. In MBR, the GMs, such as activated carbon (AC) and Zeolite, can adsorb some foulants (ie. EPS and SMP) and adjust sludge properties [16]. Apart from adsorption behavior, as a solid GM, AC also generates a mechanical scouring stress on the membrane surface, providing the potential to better promote the membrane fouling control [17]. Moreover, AC functionalization is also expected to facilitate the membrane fouling removal. Immobilizing laccase on AC to produce the laccase immobilized activated carbon (LAC) has been proven to straighten the adsorption capacity [18]. Although the dynamic scouring, adsorption behavior and enzymatic activity of GM exert the positive effects on fouling control, their underlying mechanism and contribution for filtration performance in MBR has yet to be revealed.

To elucidate the GM multifunctional dynamic scouring mechanism for improving the filtration performance, several issues need to be resolved: 1) what is the mechanism and mathematical model for GM dynamic scouring on the membrane surface? (2) can the dynamic scouring, adsorption behavior and enzymatic degradation effectively facilitate the fouling control in MBR? (3) how to evaluate their contribution importance to enhance the filtration performance? (4) what is the optimized operating condition for GM in MBR?

To address these unknowns from the views of theory and experiment, the present work is thus to study the GM dynamic scouring mechanism, to estimate its contribution for improving the filtration performance and to reveal the influencing factors and optimized conditions. The main work contents include 1) to reveal the filtration performance of AGS-filtration process under GM addition; 2) to propose a hydrodynamic model for clarifying the GM dynamic scouring mechanism on the membrane surface; 3) to develop a new estimation method to calculate the contribution rate of dynamic scouring, adsorption behavior and enzymatic degradation, then quantify their importance for membrane fouling control; and 4) to explain the influencing factors of GM dynamic scouring and its optimized conditions in MBR. This work identifies the mechanisms underlying the GM dynamic scouring will allow the development of targeted strategies to improve the MBR fouling control.

2. Materials and methods

2.1. Experimental set-up

A dead-end filtration cell that allows flexible operation (i.e., adjustment of membrane type, TMP, and shear stress) and accurate measurement of various filtration resistances was used to simulate the AGS-filtration process. Membranes having different pore sizes (summary in Table 1) were used in the AGS-filtration tests to investigate the effect of membrane pore size on the filtration performance. TMP of 0.1, 0.2, 0.3, 0.4, and 0.5 mPa and shear stress of 0.4, 0.8, and 1.2 Pa were generated, respectively, by an external high-pressure nitrogen gas and agitator, to mimic the internal reactor condition. GMs (AC and LAC, particle size: 150–300, 300–600 and 600–1200 μm) with various concentrations were added in the AGS-filtration process. The fabrication method of LAC was described in the previous study [19]. The permeating flux was calculated based on the electronic scale that measured the weight of the permeating solution.

The AGS was cultivated in a sequencing batch reactor (SBR), subsequent to size classification via the sieving method [20], and then used for the filtration test. The same mixed liquor suspended solids concentration of 4800 mg L^{-1} of the AGS in each filtration test was maintained.

2.2. Experimental procedure

Filtration test: the short-term (5 h) and long-term filtration (60 days) tests were conducted with various added GMs, TMPs, shear stresses, and membrane types to assess the filtration performance (threshold flux, turning point of membrane fouling resistance and membrane cleaning). To reduce the effect of feeding volume, the filtration tests were done with recycling permeate. In the dynamic and static filtration tests, 0.4 mPa and MF0.3 were chosen for TMP and membrane, respectively. For the dynamic filtration test, the hydraulic shear stress was 0.4 Pa with a stirring operation. In the static filtration test, the hydraulic shear stress was 0 Pa without a stirring operation.

Membrane fouling characterization: the micromorphology of the membranes was examined via Scanning Electron Microscope (SEM, SN-3400, Hitachi Ltd., Japan) and Atomic Force Microscope (AFM, XE-100, Park System, Korea) before and after filtration. The ATR-FTIR (660-IR, Varian, Australia) was used to identify the foulant composition.

Membrane cleaning: a two-step membrane cleaning process was conducted after filtration, namely 1) the physical cleaning step when the fouled membrane was flushed with deionized water, at 300 rpm for 10 min, to remove the cake layer from the fouled membrane; and 2) the chemical cleaning step when the cleaning detergents (P3-ultrasil 10 [Ecolab, cleaning USA] concentration of 2.5 g/L and pH of 6.7) were applied for removing foulant via mixing operation, for 20 min, to remove the foulant from the membrane. Water permeability was calculated to determine the permeability recovery after each cleaning step.

Permeability recovery (%) is defined by the following equation:

$$\text{Permeability recovery} = \frac{L_{pc}}{L_{pi}} \times 100\% \tag{1}$$

where L_{pc} and L_{pi} are the water permeability values (L m^{-2} h^{-1} [LMH]) of the cleaned/fouled and new membranes, respectively.

Table 1
The properties of membranes (ANDE Co. Ltd).

Membrane	Pore size (μm)	Material	Permeability (LMH mPa^{-1})
UF020	0.02	PES	60
UF050	0.05	PES	160
MF0.1	0.1	PVDF	>500
MF0.2	0.2	PVDF	>800
MF0.3	0.3	PVDF	>900

Critical radius (r_c, m) [11] was calculated by the following equation:

$$r_c = \frac{521N}{100 + 42.5N} \tag{2}$$

where N is stirring speed (rpm).

Shear stress (τ_{av}, Pa) [11] was defined according to the following equation:

$$\tau_{av} = 0.0742N^{1.5}\left(r_c^{1.6} - 138r_c^3\right) \tag{3}$$

According to Darcy's law, a resistance-in-series model can be used to calculate the membrane fouling resistance [21]:

$$J = \frac{TMP}{\mu \cdot R_t} = \frac{TMP}{\mu \cdot (R_m + R_f)} \tag{4}$$

where μ is the viscosity of the membrane, R_t is the total filtration resistance, R_m is the intrinsic membrane resistance and R_f is the membrane fouling resistance.

2.3. Membrane filtration performance estimation

The membrane filtration performance can be evaluated by the permeability behavior and membrane fouling resistance stability. The threshold flux theory can quantitatively characterize the permeability behavior [22,23]. The membrane fouling resistance stability is investigated by the turning point of membrane fouling resistance model [24,25].

2.3.1. Threshold flux theory

Threshold flux is an indicator of fouling rate, and MBR can achieve the sustainably high flux and low fouling rate by operating at the threshold flux [26]. Threshold flux can be identified by the flux-TMP profile and linear regression [23]: a straight line of best fitting is drawn through stable flux points from the initial point to a certain point (as long as possible), and the threshold point is the last point in this regression line of best fitting. Thereby, the abscissa and ordinate of threshold point (J_{thr}, TMP_{thr}) are the threshold flux and threshold TMP, respectively.

2.3.2. Model for turning point of membrane fouling resistance

Turning point of membrane fouling resistance is a key trigger point of irreversible membrane fouling. Exceeding it, the membrane fouling resistance sharply increases, and less than it, the membrane fouling resistance slightly raises with flux. Turning point of membrane fouling resistance can be determined by the fouling resistance-flux profile [24]: the ascent rate of membrane fouling resistance exhibits a small level at low flux, then clearly elevates. Especially at the turning point, it has a transition of about 90° and the membrane fouling resistance raises in a straight line. Hence, the abscissa and ordinate of trigger point in fouling resistance-flux profile are the turning point of membrane fouling resistance.

Both threshold flux and turning point of membrane fouling resistance can indicate the fouling rate variation. In fact, the turning point of membrane fouling resistance can become the measurement method of threshold flux. Exceed them, the membrane fouling rate rapidly increases; below them, the membrane fouling rate keeps at a low value. Threshold flux shows the relationship between flux and TMP, while turning point of membrane fouling resistance displays the relationship between flux and membrane fouling resistance.

3. Results and discussion

3.1. The filtration performance of AGS-filtration process

3.1.1. The effect of membrane type

Fig. 1 (a) presents the permeate fluxes of UF and MF membranes

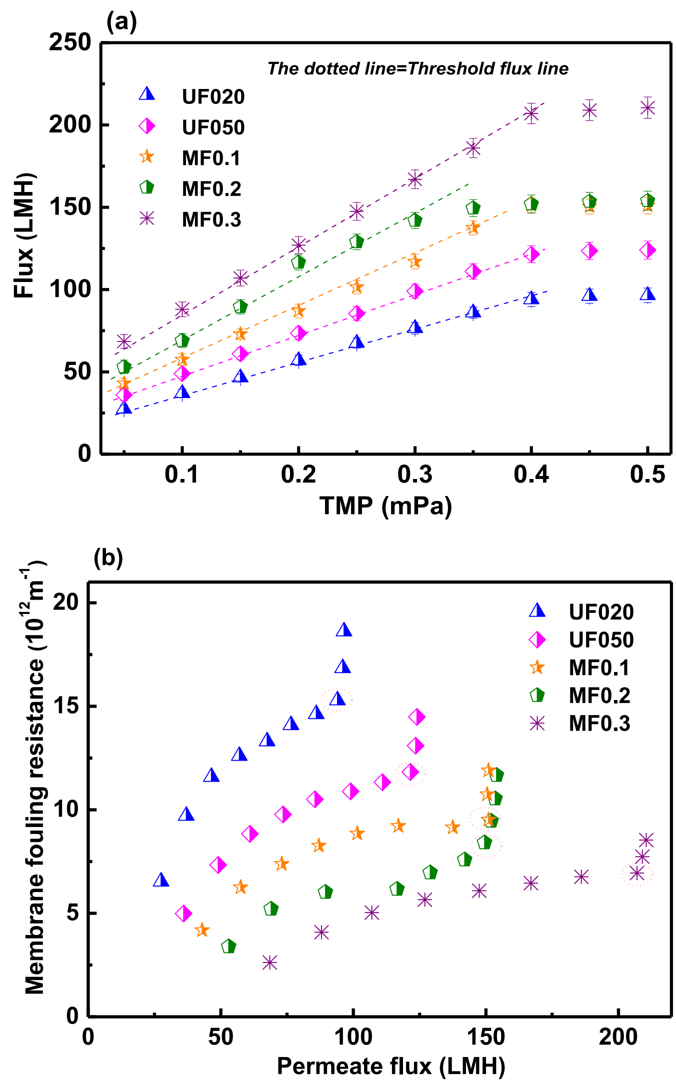

Figure 1. Flux (a) and membrane fouling resistance (b) of AGS-filtration process for short-term filtration test at different membranes (shear stress of 0.4 Pa and temperature of 25 °C).

during AGS-filtration process. As expected, at the greater membrane pore size and porosity, the permeate flux increased [24]. Meanwhile, more foulants passed through membrane with larger pore size, thus slightly decreasing membrane fouling. Thus, with respect to MF0.3, the membrane with larger pore size also had lower intrinsic filtration resistance, thus increasing the permeate flux. It was clear that the relationship between TMP and permeate flux were grouped into three stages: in the 1st stage, the flux growth trend with TMP was linear. For the 2nd stage, the flux growth line deviated from linearity, after flux achieved the threshold flux. During the 3rd stage, the flux reached the approximately steady value, which was independent with TMP. Threshold flux could be the distinction point for membrane fouling rate and the indicator for the design flux of MBR. Below it, fouling rate kept constant. Exceeding it, fouling rate was greater than the constant value. Threshold flux was calculated by a linear regression method: the linear relationship between TMP and flux was determined by linear fitting, and the ending point of the fitting line was threshold flux [23,24]. In Fig. 1 (a), the threshold fluxes (UF020: 24.6 LMH bar^{-1}, UF050: 34.7 LMH bar^{-1}, MF0.1: 39.3 LMH bar^{-1}, MF0.2: 47.3 LMH bar^{-1} and MF0.3: 51.8 LMH bar^{-1}) of all membranes are calculated, and are obviously higher than the operating flux (10–30 LMH bar^{-1}) of the conventional MBR. This implied that AGS-MBR had a superior filtration efficiency than that of the conventional MBR. As a result, the design flux of AGS-MBR can obviously exceed that of the conventional MBR, meanwhile its fouling rate keeps low.

Fig. 1 (a) depicts that the threshold flux raises with greater membrane pore size. The threshold flux was controlled by the back transport of particles [27]. During the particle transport process, Brownian, shear-induced diffusion and barrier forces exerted the dominant effects [28]. For all AGS-filtration tests, Brownian and shear-induced diffusion were the same. The barrier force consisted of solute-solute and solute-membrane interactions, which became the reason to generate the discrepancy affecting the threshold flux for various membranes. With respect to the membrane with large pore size, more small particles permeated through membrane and entered the permeate solution, then the large foulant remained on the membrane surface [29], thus the main solute-membrane interaction was the large foulant-membrane. Regarding membrane with small pore size, the foulant on the membrane surface presented a complete diameter distribution, in that its solute-membrane interaction contained the large foulant-membrane and small foulant-membrane. Thus, the membrane with small pore size demonstrated a tighter and more complex solute-membrane interactions, causing more serious adsorption fouling, pore blocking and cake layer. Therefore, the threshold flux reduced for membrane with smaller pore size. On the other hand, the threshold TMP didn't strictly conform to this law. MF0.3, MF0.1, UF050 and UF020 possessed the same threshold TMP (0.4 mPa), meanwhile MF0.2 had lower threshold TMP (0.3 mPa). This demonstrated that MF0.3, MF0.2, UF050 and UF020 could sustain at a high TMP operation with a low fouling rate. Moreover, the limiting fluxes of all 5 membranes were observed, and they varied from 72 to 210 LMH. Although the membrane with larger pore size owns lower membrane fouling in the short-term operation, it has more potential of pore blocking during the long-term operation. In the actual engineering, the effect of pore size on fouling formation is quite complicate, because the actual foulant concentration in the retentate for different membranes is distinct and the pollutant concentration in wastewater also varies with time. These may affect the growth rate of membrane fouling. Therefore, the threshold flux in the long-term operation for engineering applications should take these factors into consideration.

The relationship between permeate flux and membrane fouling resistance is displayed in Fig. 1 (b). For all membranes, along the flux increased, membrane fouling resistance elevated. At a greater permeate flux, the impetus of filtration intensified and more foulant was pushed towards membrane surface, producing more contact sites between foulant and membrane, finally leading to higher membrane fouling resistance. Furthermore, there was a turning point in the flux-fouling resistance curve. The turning point corresponds with the threshold flux point in Fig. 1 (a). Below the turning point, the membrane fouling resistance slowly enhanced. Beyond it, the membrane fouling resistance elevated rapidly. This also confirms the significance of threshold flux, while the membrane fouling resistance of threshold flux for all membranes are acquired from Fig. 1 (b): 15.3×10^{12} m^{-1} (UF020), 11.7×10^{12} m^{-1} (UF050), 9.2×10^{12} m^{-1} (MF0.1), 7.6×10^{12} m^{-1} (MF0.2) and 6.9×10^{12} m^{-1} (MF0.3). UF020 and MF0.3 possessed the highest and the lowest values, respectively, since more foulant was intercepted by UF020 with the smallest pore size. Furthermore, contrast to other membranes, MF0.3 exhibited the high filtration efficiency, which proved to be an ideal selection for AGS-MBR application. However, after outstripping the threshold flux, AGS-MBR still faced the membrane fouling control problem and needed more exploration of fouling control strategies for elevating threshold flux and diminishing the turning point of membrane fouling resistance.

3.1.2. The influence of shear stress

Fig. 2 presents the influence of shear stress on the permeate flux and membrane fouling resistance of AGS-filtration for MF0.3. Along shear stress increased, expectedly, the permeate flux improved and membrane fouling resistance curtailed, because of the diminishment of concentration polarization and membrane fouling. Moreover, the threshold flux also elevated with the enlargement of shear stress, because of the shear-induced back diffusion for AGS [30,31]. Besides, the anti-fouling capacity strengthened at higher shear stress, thus the critical point for fouling rate debated and threshold TMP also raised. In fact, even at a low shear stress (0.4 Pa) and a small shear-induced back diffusion, the permeate flux of AGS-filtration still possessed a desirable efficiency (both threshold and limiting fluxes exceeding 180 LMH). Moreover, under the stimulate of hydraulic shear, AGS encompassed the dynamic scouring for enhancing foulant removal on the membrane surface. Thus, at great TMP, membrane fouling sharply increased and a more effective fouling control strategy should be employed to improve the filtration performance.

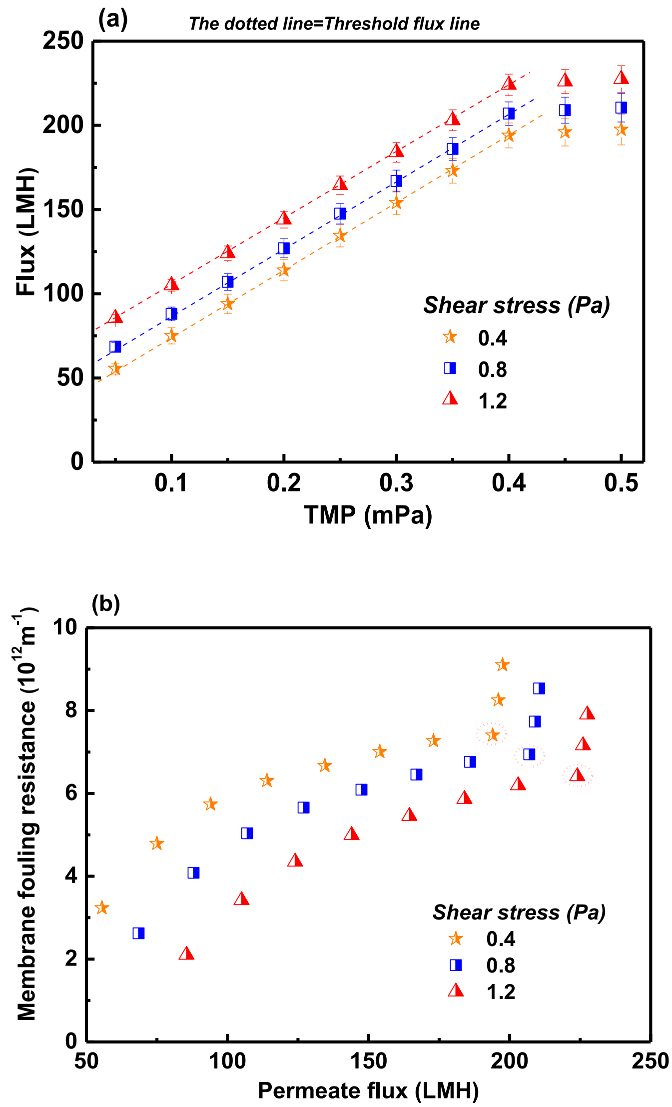

Fig. 2. Flux (a) and membrane fouling resistance and (b) of AGS-filtration process for short-term filtration test at different shear stresses (TMP of 0.4 mPa, membrane of MF0.3 and temperature of 25 °C).

3.1.3. Flux decline during long-term filtration process

Long-term filtration performance is crucial for MBR application. As illustrated in Fig. 3, when shear stress increases from 0 to 1.2 Pa, the permeate flux strongly raises (18.1 LMH→75.2 LMH at 0 Pa, 2.4 LMH→16.3 LMH at 1.2 Pa), while flux decline distinctly reduces (86.7% at 0 Pa→78.3% at 1.2 Pa). Hence the shear stress evidently promoted the

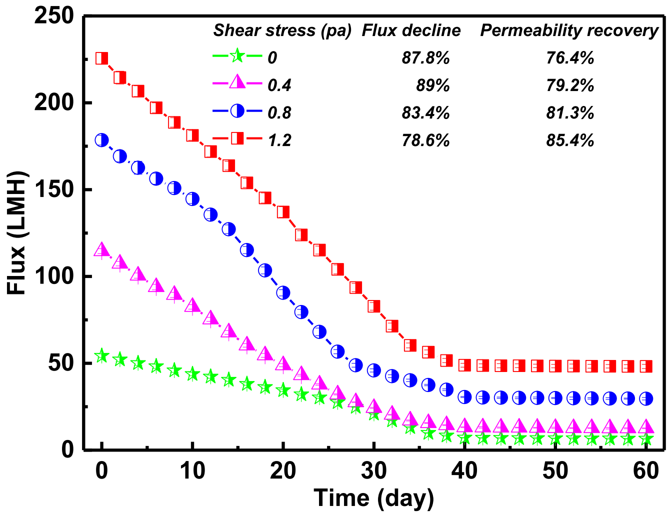

Fig. 3. Long-term filtration performance of AGS-filtration process at different shear stresses. (TMP of 0.4 mPa, shear stress of 0.4 Pa, membrane of MF0.3 and temperature of 25 °C).

permeate flux and decreased the flux decline for the long-term filtration process (60 days). This indicated that via the stronger hydraulic shear intensity, AGS dynamic scouring capacity towards membrane reinforced, offering the greater filtration performance. Moreover, the permeability recovery after membrane cleaning also strengthened with shear stress, since the greater AGS dynamic scouring produced by larger hydraulic shear stress was conducive to remove the membrane foulant and reduce the membrane fouling resistance. Nevertheless, the permeability recovery was still below 90%, demonstrating that elevating shear stress was difficult to furtherly promote the membrane cleaning efficiency, and more means needed be developed to improve the permeability recovery efficiency.

3.2. Granular material dynamic scouring enhanced filtration mechanism

For the purpose of enhancing the filtration performance, two GMs (AC and LAC) were employed in AGS-filtration process to promote the dynamic scouring effect. Fig. 4 depicts the threshold flux and turning point of membrane fouling resistance. After adding GMs, AGS-filtration process exhibited the higher threshold flux and smaller turning point of

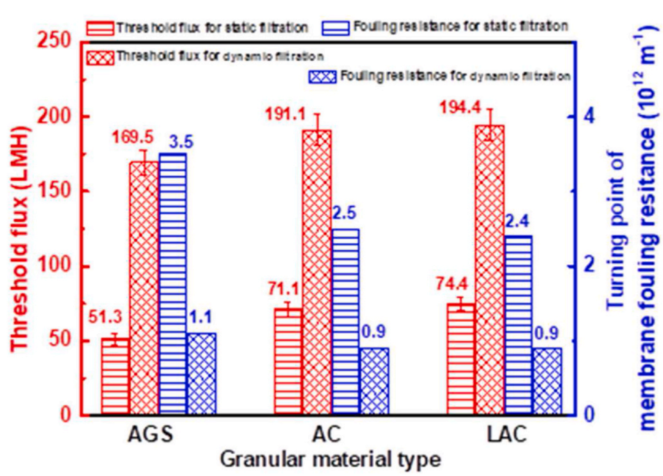

Fig. 4. Threshold flux and turning point of membrane fouling resistance for short-term filtration test under various granular materials (TMP of 0.4 mPa, shear stress of 0.4 Pa [only for dynamic filtration], membrane of MF0.3 and temperature of 25 °C).

membrane fouling resistance. During AGS filtration process, AGS displayed a non-steady shear state and showed a collision effect on the membrane surface in the movement process [11]. This collision and friction between AGS and membrane created a dynamic scouring and exerted an additional force on the membrane surface, thus increasing the shear stress on the membrane surface [17]. Theoretically, the dynamic scouring mechanism was in the light of the momentum transferred from the AGS or GMs to foulants. The dynamic scouring stress, derived from the collision and friction between GM and membrane, was produced by momentum conservation [11] and could be conceptualized in the following formula:

$$DSS \propto d_{GM}^{3} \bullet N_{GM} \bullet t \tag{5}$$

where DSS is the dynamic scouring stress, d_{GM} is the GM diameter, N_{GM} is the total number of GM, and t is the filtration time.

Dynamic scouring stress was proportional to the GM diameter, total number of GM, and filtration time. After linear fitting, the dynamic scouring stress model could be formulated as follow:

$$DSS = k \bullet d_{GM}^{3} \bullet N_{GM} \bullet t = k \bullet V_{GM} \bullet t \tag{6}$$

where k is the dynamic scouring coefficient and V_{GM} is the total mass of GM.

Dynamic scouring stress was proportional to the total mass of GM, and the greater mass produced a stronger dynamic scouring stress. The GM addition held a dynamic scouring towards membrane. The larger total mass of GM, more opportunities for collisions and friction, and more intense dynamic scouring occurred. The effect of granular material size had a certain effect on dynamic scouring efficiency (seen in Supplementary File). Besides, the dynamic scouring coefficient may be affected by the granular material, and the mechanism needs to be furtherly studied in the future. Thus, the shear stress enhanced under the dynamic scouring of GM, then straightened the membrane fouling control, leading to higher threshold flux and lower turning point. On the other hand, the GM property was another critical influencing factor for fouling control. First, compared with AGS, the AC displayed a greater density and harder structure [20], and these properties brought about the stronger collision momentum exchange process and frictional shear rate with membrane, accelerating momentum transfer between GM and foulants. Second, AC was able to absorb the colloidal substances and EPS [32,33], then limited the adhesion of major foulants to the membrane surface. Third, as the upgraded version of AC, LAC was endowed with enzymatic degradation function [34]. The synergy of adsorption behavior and enzymatic degradation improved the foulant removal efficiency. Besides, the dynamic scouring also elevated the adsorption behavior and enzymatic degradation by promoting the collision frequent between GM and foulants. On the other hand, the mechanical stability of membrane offered a dynamic scouring wall surface for GM strong behavior, then obviously straightening the collision and friction between GM and membrane, afterward promoting the GM dynamic scouring effect. In addition, AC was mixed with the sludge in the cake layer to reduce the filtration resistance. To sum up, the optimized order of filtration performance was LAC > AC > AGS, due to the multifunctional synergy.

The micromorphology of the fouled membrane under various GM addition for different filtration state was characterized by SEM and AFM (seen in Fig. 5). After a long-term filtration, the AGS foulant deposited, and foulant accumulated on the membrane surface, then a clear cake layer formed (Fig. 5 b). Under the AC and LAC addition, the relatively porous and loose fouling layer appeared (Fig. 5 c and f) in the static filtration, since the mixture of AC/LAC in the cake layer raised the porosity. As for the dynamic filtration, the strong dynamic scouring and collision between the AC/LAC and membrane occurred, reducing the deposition of foulant on the membrane surface (Fig. 5 d and f). In compassion with AC (Fig. 5 c and d), LAC (Fig. 5 e and f) exhibited the loose structure for membrane fouling, on account of the enzymatic

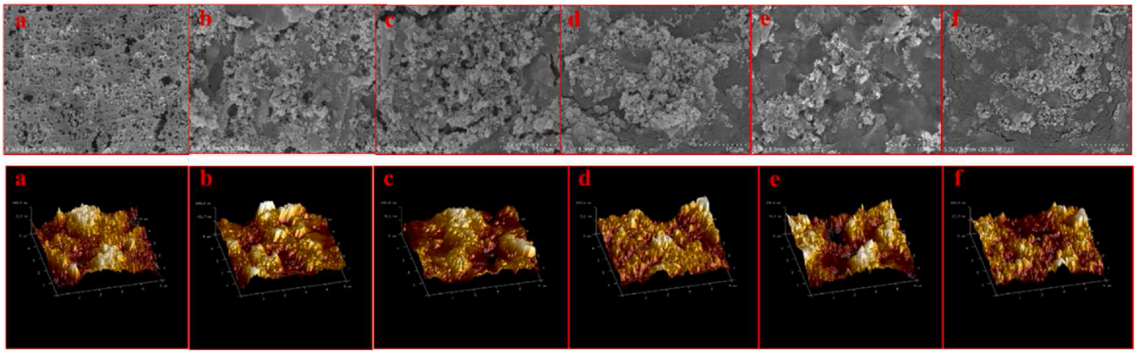

Fig. 5. The SEM and AFM images of the membrane: (a) new membrane, (b) AGS fouled membrane, (c) AC fouled membrane at static filtration, (d) AC fouled membrane at dynamic filtration, (e) LAC fouled membrane at static filtration, and (f) LAC fouled membrane at dynamic filtration.

degradation. Furthermore, the AFM images that showed the vertical distribution of foulants on the membrane surface at various GMs are presented in Fig. 5. At AGS-filtration process, the AGS formed a rough fouling layer on the membrane surface (Fig. 5 b). As the AC/LAC addition, the membrane surface roughness decreased (Fig. 5 c and d) because of less foulant adhering to the membrane surface by the synergy of adsorption behavior and enzymatic degradation. Compared with the static filtration (Fig. 5 c and e), the dynamic filtration (Fig. 5 d and e) obviously removed the foulant depositing and accumulating on the membrane surface, diminishing membrane surface roughness. For LAC (Fig. 5 c and d), the enzymatic degradation elevated the foulant removal, thus the foulant existing on the membrane surface reduced and the membrane surface became smoother than AC (Fig. 5 d and f). Hence, it is concluded that the GM multifunctional dynamic scouring improves the foulant removal.

3.3. The contribution evaluation model for dynamic scouring, adsorption behavior, and enzymatic degradation

Dynamic scouring, adsorption behavior and enzymatic degradation have been proven to effectively improve the filtration performance, however their comprehensive understanding for contribution rate of various GM functions is still lacking. To comprehend the contribution rates of dynamic scouring, adsorption behavior, and enzymatic degradation to improve the filtration performance after adding GM, based on the changes of membrane fouling resistances at dynamic and static filtrations, a contribution evaluation model for filtration performance improvement was proposed in this section.

At first, some reasonable assumptions are made: 1) dynamic scouring, including GM dynamic scouring and AGS dynamic scouring, occurs both near and on the membrane surface, thus it simultaneously affects the concentration polarization and membrane fouling layer; 2) given the large adsorption capacity and enough reactive time proved by slow filtration rate at static filtration, the adsorption behavior and enzymatic degradation can play a desirable role in static filtration, and the effects are equivalent to the dynamic filtration; 3) AC and LAC exhibit the great water permeability, and the filtration resistance forming in the static filtration can be ignored. Furthermore, as shown in Fig. 4, the membrane fouling resistances before and after GM addition at both the dynamic and static filtrations are summarized.

The contribution rate of adsorption behavior (C_A) can be expressed by the reduction rate between AC and AGS membrane fouling resistance under the static filtration.

$$C_A = \frac{R_{AGS,\,s} - R_{AC,s}}{R_{AGS,\,s} - R_{LAC,d}} \times 100\% \tag{7}$$

where $R_{AGS,\,s}$ and $R_{AC,s}$ are the AGS and AC membrane fouling resistance under the static filtrations, respectively.

The contribution rate of enzymatic degradation (C_{ED}) can be expressed by the reduction rate between AC and LAC membrane fouling resistance under the static filtration.

$$C_{ED} = \frac{R_{AC,s} - R_{LAC,s}}{R_{AGS,\,s} - R_{LAC,d}} \times 100\% \tag{8}$$

where $R_{BAC,s}$ is the LAC membrane fouling resistance under the static filtration.

The contribution rate of dynamic scouring (C_{DS}) is calculated by 100% subtracting C_A and C_{ED}:

$$C_{DS} = 100\% - C_{ED} - C_A \tag{9}$$

Fig. 4 displays that after GM addition, the membrane fouling resistances obviously reduce as follow: AGS (1.1 × 10^{-12} m^{-1} [dynamic filtration] and 3.5 × 10^{-12} m^{-1} [static filtration]) → AC (0.9 × 10^{-12} m^{-1} [dynamic filtration] and 2.5 × 10^{-12} m^{-1} [static filtration]) → LAC (0.9 × 10^{-12} m^{-1} [dynamic filtration] and 2.4 × 10^{-12} m^{-1} [static filtration]), respectively, because membrane fouling can be effectively reduced by the dynamic scouring, adsorption behavior, and enzymatic degradation. Fig. 6 presents that their contribution rates are 59.1%, 36.4% and 4.6%, respectively. The largest contribution rate was dynamic scouring (59.1%). The addition of AGS, AC and LAC generated the intensive dynamic scouring stress for removing membrane foulants, while produced the collision with foulants to reduce foulant deposition by momentum exchange. Moreover, the addition of AC and LAC clearly increased dynamic scouring stress via raising the total mass of GM, thus gradually diminishing the membrane fouling resistance. On the other hand, the mechanical stability of GM also furtherly improved the

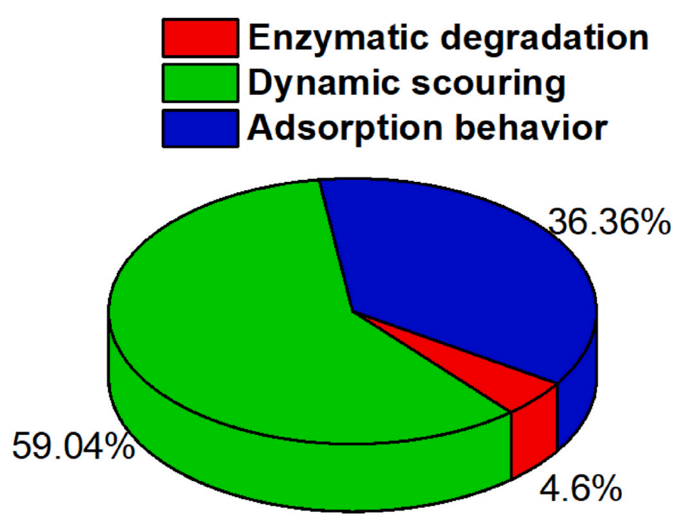

Fig. 6. The contribution rates to improve the filtration performance by granular material.

dynamic scouring. Additionally, the dynamic scouring also generated the local turbulence near the membrane surface.

The second one was the adsorption behavior (36.4%). AC and LAC absorbed the EPS, SMP and other membrane foulant, thus reducing the filtration resistance. At the same time, the dynamic scouring promoted the GM movement, and enhanced the colloid opportunities between GM and foulants, then straightening the adsorption efficiency.

The last one was enzymatic degradation (4.6%), under which, the foulant could be biocatalytic degraded by laccase immobilizing on AC. Meanwhile, the foulant adsorbed on AC also degraded, thus the adsorption capacity enhanced. Dynamic scouring showed a tremendous help for fouling control. Especially for the GM addition, its high mass improved the dynamic scouring. Except for dynamic scouring, the GM also offered the desirable adsorption behavior for removing the small organic matter which easily caused the serious membrane fouling. In term of enzymatic degradation, although its contribution was not prominent, it still pointed to a promising direction for future improvement. In a word, the GM dynamic scouring produces a multifunctional synergistic effect to promote the filtration performance in MBR.

3.4. Filtration performance at various granular material concentrations

During AGS-filtration process, the GM concentration can enhance the dynamic scouring strength, then exert a clear influence on the filtration performance. To that end, the AC and LAC at various concentrations were added into the AGS-filtration process. As shown in Fig. 7 (a) and (b), at higher GM concentration (0 → 8 g/L), the threshold flux gradually raises and the turning point of membrane fouling resistance obviously decreases. First, more GM in AGS-filtration process generated the stronger AGS dynamic scouring, effectively decreasing the cake layer and pore blocking. Second, the AC and LAC possessed the great foulant removal capacity using the adsorption behavior and enzymatic degradation. Third, the dynamic scouring also accelerated the GM movement and collision between GM and foulants, afterward strengthened the adsorption rate. On the other hand, the membrane provided a stable support surface for the movement, collision and friction of high-concentration GM on the membrane surface, thereby GM could exert a better dynamic scouring. Moreover, the GM forming the additional filtration layer on the membrane surface [35], played a secondary rejection capacity for enhancing foulant removal ability. Afterthat, the mixture of AC/LAC and foulants at larger AC/LAC concentration displayed a high porosity and smaller filtration resistance. Thus, the addition of AC and LAC clearly improved the threshold flux and reduced the irreversible fouling. However, when the GM concentration reached 12 g/L, the threshold flux diminished and turning point of membrane fouling resistance elevated, due to the enlargement of filtration resistance caused by more GM depositing on the membrane surface. Meanwhile, the excessive GM concentration brought about the overcrowding behavior of GM on the membrane surface, which was not conducive to the dynamic scouring, adsorption behavior and enzymatic degradation. Besides, the dynamic filtration displayed a much higher threshold flux than the static filtration, since the hydraulic shear stress facilitated the dynamic scouring stress intensity for promoting fouling control. In addition, as the upgraded AC, LAC owned the greater adsorption capacity on account of the enzymatic degradation of laccase.

The effect of GM addition on the membrane cleaning is presented in Fig. 7 (c). With the increase of GM concentration, the permeability recovery elevated until 8 g/L and exceeded 90%. The GM exerted a positive effect on the irreversible foulant removal by the dynamic scouring, adsorption behavior and enzymatic degradation. AGS and GM produced the dynamic scouring on the membrane surface for reducing the pore blocking, while AC absorbed the irreversible foulants, as well as the laccase immobilizing on GM catalyzed the irreversible foulant degradation [36]. The synergistic effect of these mechanisms contributed the irreversible fouling decrement, then elevated the permeability recovery after membrane cleaning. Nevertheless, once the granular material

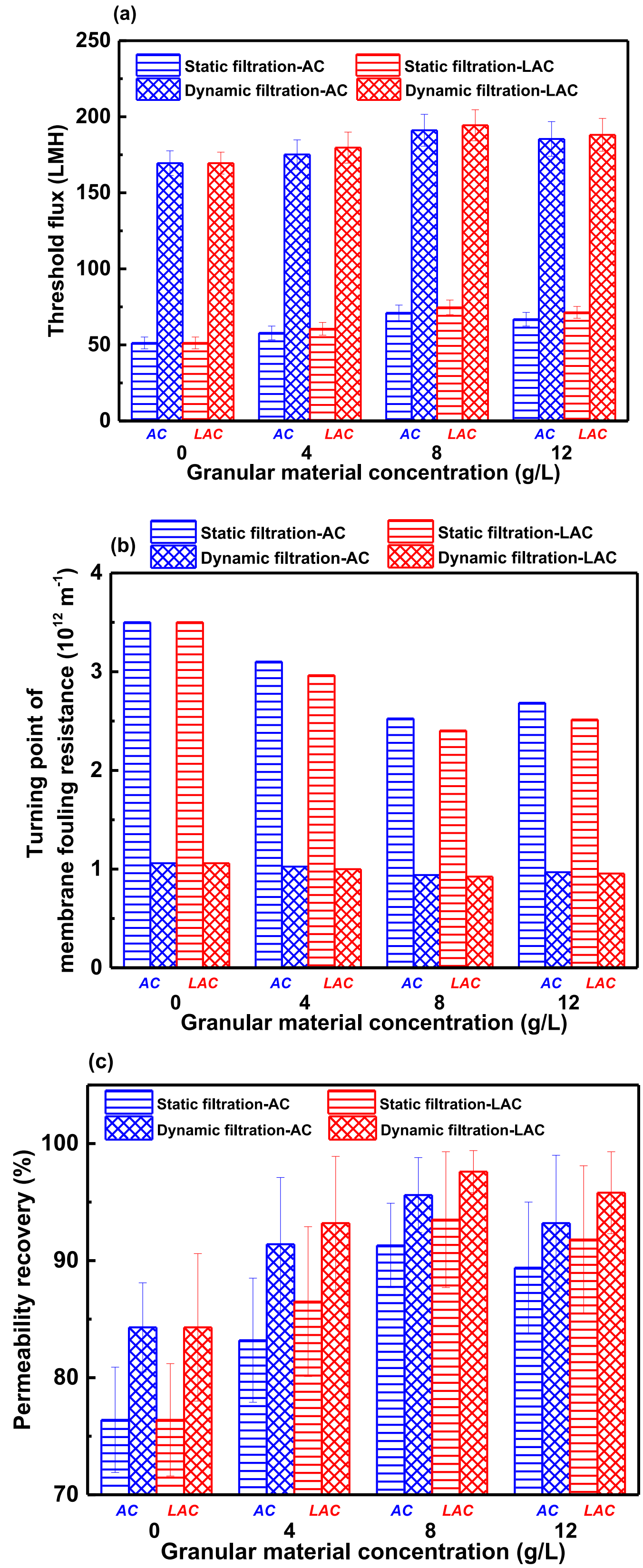

Fig. 7. The effect of granular material concentration on (a) threshold flux, (b) turning point of membrane fouling resistance and (c) membrane cleaning for short-term filtration test (TMP of 0.4 mPa, shear stress of 0.4 Pa [only for dynamic filtration], membrane of MF0.3 and temperature of 25 °C).

concentration exceeded 8 g/L, the membrane cleaning efficiency decreased, since the overcrowding behavior of GM caused by high GM concentration weakened the dynamic scouring, adsorption behavior, and enzymatic efficiency. To sum up, 8 g/L is the optimized GM concentration for the improving the filtration performance.

3.5. Discussion on dynamic scouring enhanced AGS-MBR filtration performance

As an upgraded version of activated sludge, AGS exhibits the advantage for organic and nutrient removal as well as process design. AGS-MBR is the integration of AGS and membrane technology. In this work, the threshold and limiting fluxes for MF0.3 during AGS-filtration process exceed 169 and 207 LMH, even under a very low hydraulic shear stress (0.4 Pa). Thus, the operating flux of AGS-MBR can outstrip 150 LMH, which is obviously greater than that of the conventional MBR (10–30 LMH). Meanwhile, the analysis of comprehensive membrane fouling mechanisms reveals that AGS-MBR possesses a considerably lower membrane fouling than that of the conventional MBR. Moreover, via adding GM, the threshold flux rises to 194 LMH, indicating that AGS-MBR still owns room for further improvement. Besides, others previous studies (seen in Table 2) also prove that AGS-MBR demonstrates an excellent antifouling capacity. However, AGS owns an instability during the long-term operation, especially for the hydrodynamic environment in the conventional MBR. As we all know, SBR can provide a stable living environment for AGS. Integrating SBR and MBR may become a desired solution. With the reasonable design of SBR-MBR, AGS can stably exist and membrane keeps a low membrane fouling degree. Thus, both AGS stability and membrane fouling are expected to be solved at the same time.

4. Conclusions

The current study revealed the GM dynamic scouring mechanism, clarified the multifunctional quantitative evaluation, and explained the filtration performance at various GM operating conditions in MBR. The following conclusions can be made:

* AGS-filtration process was limited by the presence of irreversible membrane fouling, decreasing the filtration performance in MBR (threshold flux [169.5 LMH] and (turning point of membrane fouling resistance [1.1×10^{12} m^{-1}]).
* The GMs (AC and LAC) were added into AGS-filtration process to promote the dynamic scouring and endow the novel functions (adsorption behavior and enzymatic degradation) for improve the filtration performance.
* According to the momentum conservation, the dynamic scouring model was developed to calculate the dynamic scouring stress, which was proportional to the total mass of GM on the membrane surface. The stable mechanical structure of the membrane provided a stronger support for the movement, friction and collision of GM on the membrane surface, thus promoting the dynamic scouring.
* A new contribution quantification model was proposed for evaluating the contribution rates of dynamic scouring (59.1%), adsorption behavior (36.4%) and enzymatic degradation (4.6%), implying that the dynamic scouring and adsorption behavior brought about the dominated promotion.
* At the GM concentration of 8 g/L and size of 300–600 μm, AGS-filtration process exhibited an optimized performance in term of threshold flux, turning point of membrane fouling resistance and membrane cleaning.

Table 2
AGS-MBRs performance.

Reactor structure	Membrane	Operating flux (LMH)	TMP	Pollutant concentration	Pollutant removal	AGS size and stability	Reference
Cylindrical reactor (30 cm inside diameter, 19.8, 26.4 and 33 L volume, and 1.23 cm/s air rising velocity)	PVDF, pore diameter: 0.15 μm, and effective area: 0.264 m^2	12.5	TMP 0 → 0.5 mPa 1st cycle: 0–15 days 2nd cycle: 15–125 days 3rd cycle: 125–180 days	COD = 500–800 mg L^{-1}	R_{TOC} = 98 ± 1% $R_{NH3\text{-}N}$ = 97%	Mean size: 517 ± 28 μm; AGS aging after 180 days	[37]
Cylindrical reactor (30 cm inside diameter, 19.8, 26.4 and 33 L volume, and 1.23 cm/s air rising velocity)	PVDF, pore diameter: 0.15 μm, and effective area: 0.264 m^2	12.5		COD = 298–790 mg L^{-1}	R_{COD} = 96%	Mean size: 517 ± 28 μm; AGS aging after 180 days	[38]
Cylindrical reactor (6 cm inside diameter, and 2.24 L volume)	PVDF, pore diameter: 0.1 μm, and effective area: 0.025 m^2	12	TMP 0 → 0.6 mPa 1st cycle: 40–60 days 2nd cycle: 60–80 days 3rd cycle: 80–100 days 4th cycle: 100–120 days 5th cycle: 120–135 days 6th cycle: 135–155 days	COD = 1330 mg L^{-1}	R_{COD} = 99%	Mean size: 723 μm.	[39]
Cylindrical reactor (15 cm inside diameter, 19 L volume and H/D = 8)	PVDF, pore diameter: 0.1 μm, and effective area: 0.014 m^2	×	×	COD = 2902 ± 129.5 mg L^{-1}; TN = 74.53 ± 4.12 mg L^{-1}	R_{COD} = 98% R_{TN} = 96–99%	Mean size: 576 μm.	[40]
Cylindrical reactor (4 L volume)	Nylon mesh, pore diameter: 70 μm, and effective area: 0.02 m^2	0.6 L/h	TMP stabilizes at 0.2 mPa for 30 days.	COD = 400 mg L^{-1}	R_{COD} = 91.4%	Mean size: 500 μm; AGS slightly disintegrates in the start-up stage.	[41]
AGS-MBR	Microfiltration membrane, pore diameter: 0.3 μm.	135	0.2 mPa	×	×	0.2–2.0 mm	This study

× No data.

The information presented in this work will undoubtedly benefit research on the fouling control of membrane water treatment.

Author statement

Wenxiang Zhang: Investigation, Visualization, Writing-original draft, Writing-review & editing. Wenzhong Liang: Software, Visualization, Writing-original draft, formal analysis. Zhien Zhang: Software, Formal analysis.

Declaration of competing interest

The authors declare that they have no known competing financial interests or personal relationships that could have appeared to influence the work reported in this paper.

Data availability

Data will be made available on request.

Acknowledgments

The authors would like to acknowledge the financial support from the Natural Science Foundation of China (22178136 and 51908136).

Appendix A. Supplementary data

Supplementary data to this article can be found online at https://doi.org/10.1016/j.memsci.2022.120979.

References

[1] F. Meng, S. Zhang, Y. Oh, Z. Zhou, H.S. Shin, S.R. Chae, Fouling in membrane bioreactors: an updated review, Water Res. 114 (2017) 151.
[2] Y. Shi, J. Huang, G. Zeng, Y. Gu, Y. Chen, Y. Hu, B. Tang, J. Zhou, Y. Yang, L. Shi, Exploiting extracellular polymeric substances (EPS) controlling strategies for performance enhancement of biological wastewater treatments: an overview, Chmosphere 180 (2017) 396–411.
[3] W. Naessens, T. Maere, N. Ratkovich, S. Vedantam, I. Nopens, Critical review of membrane bioreactor models–part 2: hydrodynamic and integrated models, Bioresour. Technol. 122 (2012) 107–118.
[4] Z. Yang, Y. Zhou, Z. Feng, X. Rui, T. Zhang, Z. Zhang, A review on reverse osmosis and nanofiltration membranes for water purification, Polym. Bull. (Berlin) 11 (2019) 1252.
[5] Z. Wang, J. Ma, C.Y. Tang, K. Kimura, Q. Wang, X. Han, Membrane cleaning in membrane bioreactors: a review, J. Membr. Sci. 468 (2014) 276–307.
[6] B. Wang, K. Zhang, R.W. Field, Novel aeration of a large-scale flat sheet MBR: a CFD and experimental investigation, AIChE J. 64 (2018) 2721–2736.
[7] M. Yang, M. Liu, D. Yu, J. Zheng, Z. Wu, S. Zhao, J. Chang, Y. Wei, Numerical simulation of scaling-up for AEC-MBRs regarding membrane module configurations and cyclic aeration modes, Bioresour. Technol. 245 (2017) 933–943.
[8] I. Ruigómez, E. González, S. Guerra, L.E. Rodríguez-Gómez, L. Vera, Evaluation of a novel physical cleaning strategy based on HF membrane rotation during the backwashing/relaxation phases for anaerobic submerged MBR, J. Membr. Sci. 526 (2017) 181–190.
[9] I. Koyuncu, R. Sengur-Tasdemir, M.E. Ersahin, H. Ozgun, B. Kose-Mutlu, T. Turken, R. Kaya, B. Yavuzturk-Gul, 5 - applications of ceramic membrane bioreactors in water treatment, in: A. Basile, K. Ghasemzadeh, E. Jalilnejad (Eds.), Current Trends and Future Developments on (Bio-) Membranes, Elsevier, 2020, pp. 141–176.
[10] M.B. Asif, Z. Zhang, Ceramic membrane technology for water and wastewater treatment: a critical review of performance, full-scale applications, membrane fouling and prospects, Chem. Eng. J. 418 (2021), 129481.
[11] W. Zhang, W. Liang, Z. Zhang, T. Hao, Aerobic granular sludge (AGS) scouring to mitigate membrane fouling: performance, hydrodynamic mechanism and contribution quantification model, Water Res. 188 (2021), 116518.
[12] M. Sajjad, K.S. Kim, Influence of Mg2+ catalyzed granular sludge on flux sustainability in a sequencing batch membrane bioreactor system, Chem. Eng. J. 281 (2015) 404–410.
[13] R. Campo, C. Lubello, T. Lotti, G. Di Bella, Aerobic granular sludge-membrane BioReactor (AGS-MBR) as a novel configuration for wastewater treatment and fouling mitigation: a mini-review, Membranes 11 (2021) 261.
[14] A. Anantharaman, Y. Chun, T. Hua, J.W. Chew, R. Wang, Pre-deposited dynamic membrane filtration-A review, Water Res. 173 (2020), 115558.
[15] S. Wei, L. Du, S. Chen, H. Yu, X. Quan, Electro-assisted CNTs/ceramic flat sheet ultrafiltration membrane for enhanced antifouling and separation performance, Front. Environ. Sci. Eng. 15 (2021) 1–11.
[16] O.T. Iorhemen, R.A. Hamza, J.H. Tay, Membrane fouling control in membrane bioreactors (MBRs) using granular materials, Bioresour. Technol. 240 (2017) 9–24.
[17] J. Wang, A. Cahyadi, B. Wu, W. Pee, A.G. Fane, J.W. Chew, The roles of particles in enhancing membrane filtration: a review, J. Membr. Sci. 595 (2020), 117570.
[18] W. Zhou, W. Zhang, Y. Cai, Laccase immobilization for water purification: a comprehensive review, Chem. Eng. J. 403 (2020), 126272.
[19] Z. Zhu, Z. Chen, X. Luo, W. Liang, S. Li, J. He, W. Zhang, T. Hao, Z. Yang, Biomimetic dynamic membrane (BDM): fabrication method and roles of carriers and laccase, Chemosphere 240 (2020), 124882.
[20] W. Zhang, F. Jiang, Membrane fouling in aerobic granular sludge (AGS)-membrane bioreactor (MBR): effect of AGS size, Water Res. 157 (2018) 445–453.
[21] S. Meng, R. Wang, K. Zhang, X. Meng, W. Xue, H. Liu, D. Liang, Q. Zhao, Y. Liu, Transparent exopolymer particles (TEPs)-associated protobiofilm: a neglected contributor to biofouling during membrane filtration, Front. Environ. Sci. Eng. 15 (2021) 1–10.
[22] J. Luo, L. Ding, Y. Wan, M.Y. Jaffrin, Threshold flux for shear-enhanced nanofiltration: experimental observation in dairy wastewater treatment, J. Membr. Sci. 409–410 (2012) 276–284.
[23] W. Zhang, L. Ding, Z. Zhang, J. Wei, M.Y. Jaffrin, G. Huang, Threshold flux and limiting flux for micellar enhanced ultrafiltration as affected by feed water: experimental and modeling studies, J. Clean. Prod. 112 (2016).
[24] J. Luo, S.T. Morthensen, A.S. Meyer, M. Pinelo, Filtration behavior of casein glycomacropeptide (CGMP) in an enzymatic membrane reactor: fouling control by membrane selection and threshold flux operation, J. Membr. Sci. 469 (2014) 127–139.
[25] Z. Zhu, Z. Chen, X. Luo, W. Zhang, S. Meng, Gravity-driven biomimetic membrane (GDBM): an ecological water treatment technology for water purification in the open natural water system, Chem. Eng. J. 399 (2020), 125650.
[26] R.W. Field, G.K. Pearce, Critical, sustainable and threshold fluxes for membrane filtration with water industry applications, Adv. Colloid. Interfac. 164 (2011) 38.
[27] J. Luo, Z. Zhu, L. Ding, O. Bals, Y. Wan, M.Y. Jaffrin, E. Vorobiev, Flux behavior in clarification of chicory juice by high-shear membrane filtration: evidence for threshold flux, J. Membr. Sci. 435 (2013) 120–129.
[28] S. Zhao, Z. Tao, L. Chen, M. Han, B. Zhao, X. Tian, L. Wang, F. Meng, An antifouling catechol/chitosan-modified polyvinylidene fluoride membrane for sustainable oil-in-water emulsions separation, Front. Environ. Sci. Eng. 15 (2021) 1–11.
[29] S. Meng, R. Wang, X. Meng, Y. Wang, W. Fan, D. Liang, M. Zhang, Y. Liao, C. Tang, Reaction heterogeneity in the bridging effect of divalent cations on polysaccharide fouling, J. Membr. Sci. 641 (2022), 119933.
[30] Y. Zheng, W. Zhang, B. Tang, J. Ding, Y. Zheng, Z. Zhang, Membrane fouling mechanism of biofilm-membrane bioreactor (BF-MBR): pore blocking model and membrane cleaning, Bioresour. Technol. 250 (2017) 398–405.
[31] L. Wang, W. Liang, W. Chen, W. Zhang, J. Mo, K. Liang, B. Tang, Y. Zheng, F. Jiang, Integrated aerobic granular sludge and membrane process for enabling municipal wastewater treatment and reuse water production, Chem. Eng. J. 337 (2017) 300–311.
[32] X. Yu, T. Lin, H. Xu, H. Tao, W. Chen, Ultrafiltration of up-flow biological activated carbon effluent: extracellular polymer biofouling mechanism and mitigation using pre-ozonation with H2O2 backwashing, Water Res. 186 (2020), 116391.
[33] S. Meng, X. Meng, W. Fan, D. Liang, L. Wang, W. Zhang, Y. Liu, The role of transparent exopolymer particles (TEP) in membrane fouling: a critical review, Water Res. 181 (2020), 115930.
[34] W. Zhang, Q. Yang, Q. Luo, L. Shi, S. Meng, Laccase-Carbon nanotube nanocomposites for enhancing dyes removal, J. Clean. Prod. 242 (2020) 118421–118425.
[35] G.S. Ajmani, H.H. Cho, T.E.A. Chalew, K.J. Schwab, J.G. Jacangelo, H. Huang, Static and dynamic removal of aquatic natural organic matter by carbon nanotubes, Water Res. 59 (2014) 262–270.
[36] L.N. Nguyen, F.I. Hai, J. Kang, W.E. Price, L.D. Nghiem, Removal of trace organic contaminants by a membrane bioreactor–granular activated carbon (MBR-GAC) system, Bioresour. Technol. 113 (2012) 169–173.
[37] O.T. Iorhemen, R.A. Hamza, M.S. Zaghloul, J.H. Tay, Aerobic granular sludge membrane bioreactor (AGMBR): extracellular polymeric substances (EPS) analysis, Water Res. 156 (2019) 305–314.
[38] O.T. Iorhemen, R.A. Hamza, Z. Sheng, J.H. Tay, Submerged aerobic granular sludge membrane bioreactor (AGMBR): organics and nutrients (nitrogen and phosphorus) removal, Bioresource. Technol. Rep. 6 (2019) 260–267.
[39] J.H. Tay, P. Yang, W.Q. Zhuang, S.T.L. Tay, Z.H. Pan, Reactor performance and membrane filtration in aerobic granular sludge membrane bioreactor, J. Membr. Sci. 304 (2007) 24–32.
[40] O.T. Iorhemen, R.A. Hamza, M.S. Zaghloul, J.H. Tay, Simultaneous organics and nutrients removal in side-stream aerobic granular sludge membrane bioreactor (AGMBR), J. Water Proc. Eng. 21 (2018) 127–132.
[41] W. Li, Y. Wang, G. Sheng, Y. Gui, L. Yu, T. Xie, H. Yu, Integration of aerobic granular sludge and mesh filter membrane bioreactor for cost-effective wastewater treatment, Bioresour. Technol. 122 (2012) 22–26.